Modeling and compensating the dynamic hysteresis of piezoelectric actuators via a modified rate-dependent Prandtl–Ishlinskii model

2015 Smart Mater. Struct. 24 125006

(http://iopscience.iop.org/0964-1726/24/12/125006)

IOP Publishing Smart Materials and Structures
Smart Mater. Struct. 24 (2015) 125006 (12pp) doi:10.1088/0964-1726/24/12/125006

Modeling and compensating the dynamic hysteresis of piezoelectric actuators via a modified rate-dependent Prandtl–Ishlinskii model

Mei-Ju Yang, Chun-Xia Li, Guo-Ying Gu and Li-Min Zhu[1]

State Key Laboratory of Mechanical System and Vibration, School of Mechanical Engineering, Shanghai Jiao Tong University, Shanghai 200240, People's Republic of China

E-mail: yangmeixianglian@sjtu.edu.cn, lichunxia@sjtu.edu.cn, guguoying@sjtu.edu.cn and zhulm@sjtu.edu.cn

Received 30 May 2015, revised 23 September 2015
Accepted for publication 28 September 2015
Published 15 October 2015

Abstract

This paper presents a modified rate-dependent Prandtl–Ishlinskii (MRPI) model for the description and compensation of the rate-dependent asymmetric hysteresis in piezoelectric actuators. Different from the commonly used approach with dynamic weights or dynamic thresholds, the MRPI model is formulated by employing dynamic envelope functions into the play operators, while the weights and thresholds of the play operators are still static. By this way, the developed MRPI model has a relatively simple mathematic format with fewer parameters and easier parameter identification process. The benefit for the developed MRPI model also lies in the fact that the existing control approaches can be directly adopted with the MRPI model for hysteresis compensation in real-time applications. To validate the proposed model, an open-loop tracking controller and a closed-loop tracking controller are developed based on a dynamic hysteresis compensator, which is directly constructed with the MRPI model. Comparative experiments are carried out on a piezo-actuated nanopositioning stage. The experimental results demonstrate the effectiveness and superiority of the controllers based on the developed MRPI model compared to the controllers based on the rate-independent P–I model and the rate-dependent P–I model with dynamic weighting functions.

Keywords: piezoelectric actuators, dynamic hysteresis compensation, Prandtl–Ishlinskii model, tracking control

(Some figures may appear in colour only in the online journal)

1. Introduction

Nanopositioning stages are widely used in high-precision positioning and tracking applications [1–5], such as scanning probe microscopy, ultra-precision machine tools, and micro-/nanomanipulators. Most of these stages utilize piezoelectric actuators for actuation due to the excellent advantages of fast response, ultra-high resolution, and large stiffness. However, piezoelectric actuators suffer from the rate-dependent hysteresis, which means that when the input frequency increases, the hysteresis loop is variable and becomes larger and rounder [6, 7]. Such strong nonlinearity not only brings positioning errors to the system, but also complicates the control of piezoelectric actuators, as it leads to difficulty in modeling and even causes instability to the closed-loop controller.

The most common method to compensate for the hysteresis nonlinearity is to construct a feedforward inverse hysteresis compensator [8]. The key of this approach is to find an available hysteresis model that can precisely describe

[1] Author to whom any correspondence should be addressed.

hysteresis behaviors. Various methods have been developed to model the hysteresis of the piezoelectric actuators, such as the Preisach model [9, 10], Bouc–Wen model [11], Dahl model [12], and Prandtl–Ishlinskii (P–I) model [13–16]. However, most of these models are based on the assumption that the hysteresis is rate-independent. As a matter of fact, the hysteresis behaviors are generally rate-dependent. Thus, it is necessary to develop a rate-dependent model to capture the complicated dynamic hysteresis behavior, and many efforts have been made in the literature. Rate-dependent phenomenological models have been proposed to describe the rate-dependent hysteresis, such as the modified Preisach model [6, 7, 17], modified Bouc–Wen model [18, 19], and modified P–I (MPI) model [20–25]. The main idea of these rate-dependent phenomenological models is to introduce the input rate into the models in different ways. As an alternative, some attempts based on mathematical models have been made to characterize the rate-dependent hysteresis, such as an approximate model consisting of a variable gain and a variable time-delay [26], and a mathematical model based on a family of ellipses [27]. Intelligent methods such as the artificial neural network [28], support vector machines [29, 30], and fuzzy systems [31] have also been developed to describe the rate-dependent hysteresis. It can be seen that, nowadays, development of the rate-dependent hysteresis models is an interesting topic. However, from the literature, the results are not completely satisfactory and new approaches for modeling rate-dependent hysteresis are still being sought.

Among the hysteresis models, the P–I model (PIM) is the most widely used phenomenological model, which offers the property of simplicity and analytical inversion, making it attractive in real-time applications [13]. In this paper, a novel modified rate-dependent P–I (MRPI) model is developed to characterize the dynamic hysteresis nonlinearity of piezoelectric actuators. Different from replacing the fixed weights or thresholds of play operators with dynamic weights [20–22] or dynamic thresholds [23, 24], or employing a velocity damping model in the classical PIM [25], a new modeling approach is proposed to develop the MRPI model. In this approach, the classical/static weights and thresholds of the play operators are still utilized in the developed MRPI model, while dynamic envelope functions are introduced to replace the classical input functions of the play operators. By this way, the hysteresis loops can be determined by not only the amplitude of the input voltage but also the frequency of the input voltage. The main advantage of the developed MRPI model lies in the following facts: (1) the MRPI model has a relatively simple mathematic format with fewer parameters to describe the rate-dependent asymmetric hysteresis behavior of piezoelectric actuators; (2) the parameter identification of the MRPI model is relatively easy, because all the parameters can be identified simultaneously in one step without any post-processing; (3) available control approaches can be directly adopted with the MRPI model for hysteresis compensation in real-time applications. To validate the effectiveness of the developed MRPI model, a dynamic hysteresis compensator based on this model is developed using the direct inverse hysteresis compensation method. Simulation and experimental results on a piezo-actuated nanopositioning stage are presented. It should be noted that the direct inverse hysteresis compensation method has been reported in our previous work [32] for hysteresis compensation of piezoelectric actuators, but it was limited to the rate-independent PIM. As a continuation, this concept is extended in this paper to the rate-dependent PIM, and also utilized to verify the developed MRPI model.

The remainder of this paper is organized as follows. Section 2 contains the description of the MRPI model. Section 3 presents the structure and implementation of an inverse dynamic hysteresis compensator, and several tracking control schemes are presented. In section 4, a comparison of the performance of various tracking control schemes is performed and conclusions are summarized in section 5.

2. MRPI model

Before introducing the developed MRPI model, a modified MPI model is first reviewed in brief.

2.1. MPI model

The PIM, which is a weighted superposition of play operators, is widely used to describe the hysteresis nonlinearity due to its simplicity and analytical inversion [13]. The play operator is the basic operator of the PIM with symmetric and rate-independent properties. For any control input $v(t) \in C[0, t_E]$, where $C[0, t_E]$ is the space of continuous functions on the interval $[0, t_E]$, the output of the play operator $w(t) = F_r[v](t)$ with a threshold r can be expressed as [13]

$$\begin{aligned} w(0) &= F_r[v](0) = f_r(v(0), 0) \\ w(t) &= F_r[v](t) = f_r\big(v(t), w(t_i)\big) \end{aligned} \tag{1}$$

for $t_i \leqslant t \leqslant t_{i+1}, 1 \leqslant i \leqslant N$, with

$$f_r(v, w) = \max(v - r, \min(v + r, w)), \tag{2}$$

where $0 = t_1 < t_2 < \ldots < t_N = t_E$ is a partition of $[0, t_E]$ such that the function $v(t)$ is a monotone on each of the subintervals $[t_i, t_{i+1}]$.

Considering the fact that the piezoelectric actuators have the positive excitation nature, rather than using the play operator in (2), a one-side play (OSP) operator is adopted in this work. The OSP operator $F_{\mathrm{or}}[v](t)$ with a threshold $r \geqslant 0$ is defined as [33]

$$\begin{aligned} w(0) &= F_{\mathrm{or}}[v](0) = f_{\mathrm{or}}(v(0), 0) \\ w(t) &= F_{\mathrm{or}}[v](t) = f_{\mathrm{or}}\big(v(t), w(t_i)\big) \end{aligned} \tag{3}$$

for $t_i \leqslant t \leqslant t_{i+1}, 1 \leqslant i \leqslant N$, with

$$f_{\mathrm{or}}(v, w) = \max(v - r, \min(v, w)) \tag{4}$$

Subsequently, the classical PIM utilizes the above OSP operator $F_{\mathrm{or}}[v](t)$ to describe the relationship between the

output y_c and the input v, which can be written as [13, 33]

$$y_c(t) = H[v](t) = p_0 v(t) + \sum_{i=1}^{N} p_i F_{\mathrm{or}_i}[v](t) \tag{5}$$

where p_0 is a positive constant, p_i denotes the weighting value of the play operator with the threshold value r_i, and N is the number of the play operators.

To overcome the symmetric property of the classical PIM, a modified PIM is developed for the asymmetric hysteresis description by introducing a polynomial input function to replace the linear input function in the classical PIM. The mathematic expression of the MPI model is written as [16]

$$y_p(t) = H[v](t) = g(v(t)) + \sum_{i=1}^{N} p_i F_{\mathrm{or}_i}[v](t), \tag{6}$$

where $g(v(t)) = a_1 v^3(t) + a_2 v(t)$ is a polynomial input function with constants a_1 and a_2.

The PIMs mentioned above are the rate-independent hysteresis models due to the rate-independent play operator that the models employ. The output of the play operator is only influenced by the current input value and the past extrema of input function $v(t)$ while the derivative of the input shall not affect the shape of the output. It is for this reason that the aforementioned PIMs cannot be used to account for the rate-dependent property of the hysteresis in piezoelectric actuators. By using these models, we can characterize the hysteresis of piezoelectric actuators very well at low frequencies. However, as the frequency increases, large modeling errors occur when these models are used to describe the hysteresis. Therefore, it is necessary to develop a rate-dependent P–I hysteresis model.

2.2. MRPI model

Considering the fact that the classical play operator in the MPI model is rate-independent, a novel rate-dependent play operator is proposed in this work to construct a MRPI model, which is capable of describing the dynamic hysteresis nonlinearity of piezoelectric actuators. Observing the expression of the play operator in (2) and (4), it can be noticed that not only the threshold r, but also the input function $v(t)$ can be modified to change the characteristic of the play operator. The previous reported operators in [23, 24] focus on the modification of the threshold r with dynamic function to describe the rate-dependent behavior. They are generally applied to the two-side play operator as shown in (2). However, when a one-side play operator for practical application with positive excitation is utilized, the previous approach based on dynamic threshold will lose efficacy at the descending branch of the hysteresis loops.

In this paper, we propose an alternative approach to develop a rate-dependent play operator. Two dynamic envelope functions, which are functions of the input and its derivative, are introduced to replace the input function $v(t)$ in the ascending and descending branch of the operator, while the threshold of the operator is kept the same with the classical play operator. By this way, both the two-side play operator and the OSP operator can be utilized as the elementary operator in the PIM to describe the rate-dependent hysteresis nonlinearity with a relatively simple format and small change. Moreover, with the proper selection of the dynamic envelope functions, the proposed play operator can possess the rate-dependent and asymmetric properties simultaneously. It avoids the additional introduction of saturation operators, which may increase the complexity of parameter identification and controller implementation.

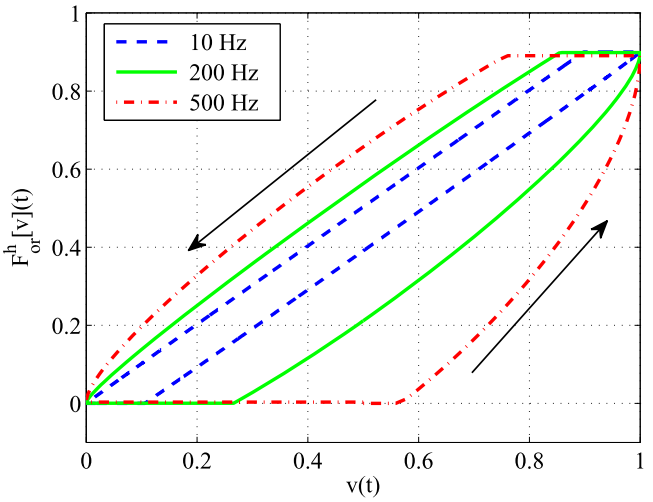

Figure 1. The input–output relationship of the rate-dependent play operator under the sinusoidal inputs with different frequencies.

Analytically, the proposed rate-dependent play operator $F^h_{\mathrm{or}}[v](t)$ with a threshold r for any control input $v(t)$ is defined as:

$$\begin{aligned} w(0) &= F^h_{\mathrm{or}}[v](0) = f^h_{\mathrm{or}}(v(0), 0) \\ w(t) &= F^h_{\mathrm{or}}[v](t) = f^h_{\mathrm{or}}\big(v(t), w(t_i)\big) \end{aligned} \tag{7}$$

for $t_i \leqslant t \leqslant t_{i+1}$,$1 \leqslant i \leqslant N$, with

$$f^h_{\mathrm{or}}(v, w) = \max\Big(h_l\big(v, \dot{v}\big) - r, \min\big(h_r\big(v, \dot{v}\big), w\big)\Big), \tag{8}$$

where $h_l(v, \dot{v})$ and $h_r(v, \dot{v})$ are the dynamic envelope functions with respect to current input $v(t)$ and its derivative $\dot{v}(t)$. The hysteresis loops between the input $v(t)$ and the output $w(t)$ are bounded by the curves h_l and h_r. The choices of these two dynamic envelope functions are not unique. These would depend on the nature of the hysteresis of the material or device. In this paper, according to the characteristic of the piezoelectric actuators, the width of the hysteresis loops becomes larger as the frequency increases. Based on this observation, the dynamic envelope functions can be selected as follows:

$$\begin{aligned} h_l\big(v(t), \dot{v}(t)\big) &= v(t) - \alpha \left|\dot{v}(t)\right| \\ h_r\big(v(t), \dot{v}(t)\big) &= v(t) + \beta \left|\dot{v}(t)\right|, \end{aligned} \tag{9}$$

where α and β are positive constants, $\dot{v}(t)$ is the derivative of the input voltage $v(t)$ which can be estimated as $\dot{v}(t) = (v(t) - v(t - T))/T$, and T is the sampling time.

The output of the proposed rate-dependent play operator based on the dynamic envelope functions in (9) is investigated under the sinusoidal inputs with different frequencies

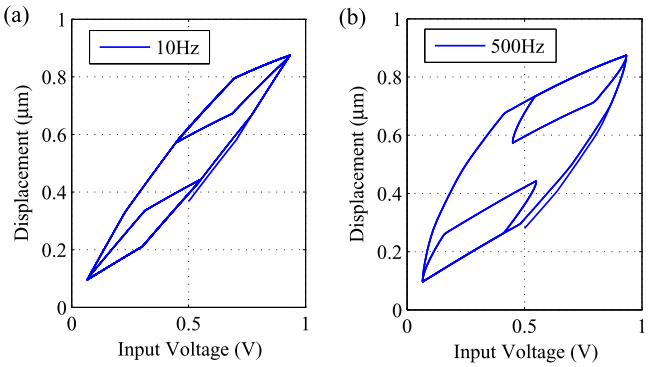

Figure 2. Hysteresis loops generated by the MRPI model.

(10, 200, and 500 Hz), while the constants in the dynamic envelope functions are selected as: $\alpha = 3 \times 10^{-4}$, $\beta = 1 \times 10^{-4}$, and the threshold r is select as 0.1. Figure 1 shows the input–output relationship of the developed rate-dependent play operator at three frequencies. The results exhibit increasing width of the hysteresis loops with increase in the frequency of the input, which demonstrates the rate-dependent property of the proposed rate-dependent play operator.

The MRPI model is subsequently formulated by integrating the proposed rate-dependent play operators, and it can be expressed as follows:

$$y_h(t) = H[v](t) = g(v(t)) + \sum_{i=1}^{N} q_i F_{\mathrm{or}_i}^{h}[v](t) \qquad (10)$$

where q_i denotes the weighting value of the rate-dependent play operator with the threshold r_i, and $g(v(t)) = b_1 v^3(t) + b_2 v(t)$ is a polynomial input function with constants b_1 and b_2. Among these parameters, b_1 influences the asymmetry of the hysteresis loop, b_2 is the approximate slope of the hysteresis loop, α and β affect the rate-dependence of the hysteresis loop, and q_i (i = 1, 2, 3, ... , N) determines the general shape of the hysteresis loops. The main advantages of the developed MRPI model can be summarized as follows: (1) compared to [20, 21, 23–25], the MRPI model has a relatively simple mathematic format with fewer parameters to describe the rate-dependent asymmetric hysteresis behavior of piezoelectric actuators, which will be investigated in section 4; (2) in contrast to [20, 25], the parameter identification of the MRPI model is simple, as all the parameters can be identified simultaneously in one step. Furthermore, as no postprocessing (e.g. curve fitting) is required, the identification of the MRPI is time-efficient. This is demonstrated in section 4.

As an illustration, an input voltage of the form $v(t) = 0.25\sin(2\pi ft) + 0.3\sin(6\pi ft) + 0.5$ is utilized to evaluate the hysteresis loops, while the fundamental frequencies are chosen as $f = 10$ and 500 Hz. Four play operators are used in this example, and the parameters of the MRPI model are selected as $b_1 = -0.0820, b_2 = 0.5, q_1 = 0.2667$, $q_2 = 0.1690, q_3 = 0.0973, q_4 = 0.1447, \alpha = 5 \times 10^{-4}$, and $\beta = 8 \times 10^{-4}$. The generated hysteresis loops at 10 and 500 Hz are given in figure 2, which shows an increase in hysteresis effect as the frequency of the input voltage increases. Therefore, the proposed hysteresis model is rate-dependent.

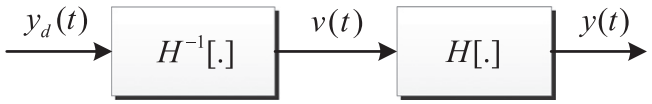

Figure 3. Block diagram of hysteresis compensation.

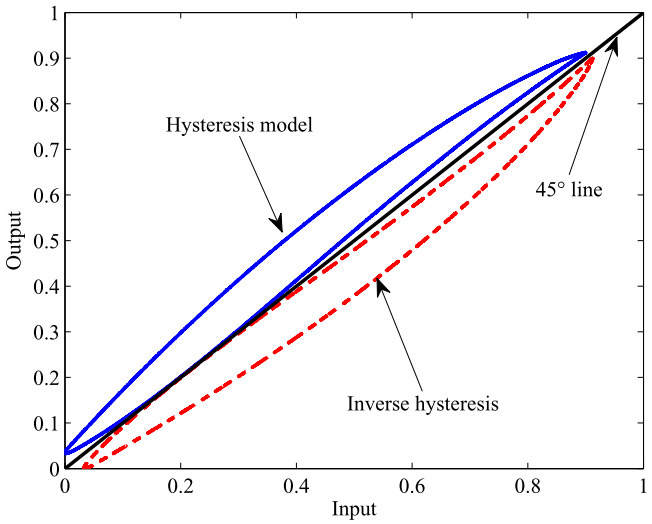

Figure 4. Relationship between the hysteresis model and its inverse model.

3. Hysteresis compensation

In this section, a direct inverse hysteresis compensator is first designed with the inverse MRPI model. Based on the compensator, open-loop and closed-loop controllers are then developed to achieve high-speed high-precision tracking control.

3.1. Direct inverse hysteresis compensator

If the hysteresis nonlinearity in piezoelectric actuators can be modeled by a hysteresis model $H[.]$, then high-precision control can be achieved for a system if an inverse hysteresis model $H^{-1}[.]$ exists such that the composition of $H[.]$ and $H^{-1}[.]$ linearizes the actuator. The block diagram of such hysteresis compensation approach is illustrated in figure 3. For a given desired trajectory $y_d(t)$, the inverse hysteresis model will generate an input signal $v(t)$ which is applied to piezoelectric actuators; the output of piezoelectric actuators is denoted as $y(t)$, which can be expressed as

$$y(t) = H\left[H^{-1}[y_d]\right](t). \qquad (11)$$

If the inverse hysteresis model $H^{-1}[.]$ is ideal, then the composite operation is linear and yields $y(t) = y_d(t)$. Therefore, the input–output relationship of the inverse hysteresis model can be directly obtained by plotting $v(t)$ against $y(t)$, whereas the hysteresis model is obtained by plotting $y(t)$

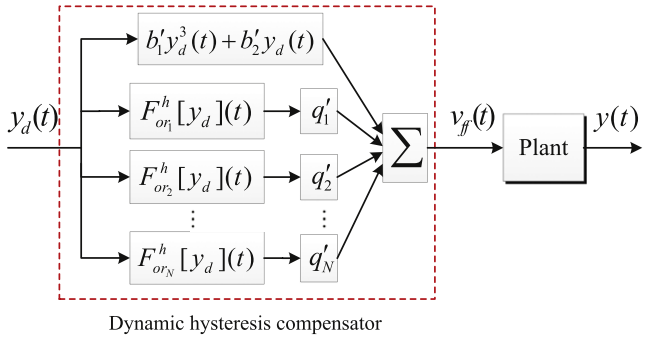

Figure 5. Block diagram of the open-loop hysteresis compensation system.

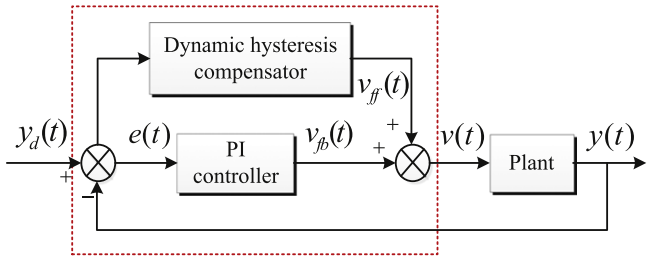

Figure 6. Block diagram of the closed-loop hysteresis compensation system.

against $v(t)$ as shown in figure 4. It can be observed that the inverse hysteresis loops and the hysteresis loops are symmetrical about the 45° line. Thus, the inverse of the PIM is also a PIM, which has been demonstrated by many researches [32, 33].

In this work, a direct inverse hysteresis compensation method, which directly applies the PIM to characterize the inverse hysteresis loops from the experimental data, is utilized to compensate for the hysteresis effect in piezoelectric actuators. By this way, both the hysteresis modeling and its complex inversion calculation are avoided. The inverse of the MPI model of (6) can be written as [32]

$$\begin{aligned} v_{ip}(t) &= H^{-1}[v](t) \\ &= a_1' y_{\mathrm{d}}^3(t) + a_2' y_{\mathrm{d}}(t) + \sum_{i=1}^{N} p_i' F_{\mathrm{or}_i}[y_{\mathrm{d}}](t), \end{aligned} \tag{12}$$

where $v_{ip}(t)$ is a compensated control voltage signal estimated by the inverse MPI model, a_1' and a_2' are the coefficients of the polynomial input function, and p_i' is the weighting value of the inverse MPI model. The validity of using the direct inverse hysteresis compensation method on the MPI model has been experimentally verified in the authors' previous work [32]. In this paper, we extend this concept to the MRPI model of (10). The inverse of the MRPI model is expressed as

$$\begin{aligned} v_{ih}(t) &= H^{-1}[v](t) \\ &= b_1' y_{\mathrm{d}}^3(t) + b_2' y_{\mathrm{d}}(t) + \sum_{i=1}^{N} q_i' F_{\mathrm{or}_i}^h[y_{\mathrm{d}}](t), \end{aligned} \tag{13}$$

where $v_{ih}(t)$ is a compensated control voltage signal estimated by the inverse MRPI model, b_1' and b_2' are the coefficients of the polynomial input function, and q_i' is the weighting value of the inverse MRPI model. In the next section, this inverse MRPI model is implemented in MATLAB for real-time tracking control.

3.2. Controller design

The main objective of tracking control is to force the output of nanopositioning stages to track a given trajectory. Once the trajectory is assigned, the determination of control signal applied to piezoelectric actuators is the target of controller design. In the following, two different control schemes are developed to generate the control signal.

3.2.1. Open-loop controller. In order to compensate for the hysteresis nonlinearity of the piezoelectric actuators, an open-loop controller based on the inverse MRPI model is first implemented. The block diagram representing the open-loop controller is shown in figure 5, where the control signal v_{ff} is obtained by (13).

3.2.2. Closed-loop controller. Due to the existence of modeling errors, the hysteresis nonlinearity cannot be totally compensated by the open-loop controller. Therefore, an additional feedback control is adopted to compensate for the model imperfection and other disturbances of the system. The block diagram of the closed-loop controller is shown in figure 6, which combines the dynamic hysteresis compensator in the feedforward loop and a proportional plus integral (PI) controller in the feedback loop. The PI controller is employed due to its robustness and ease of implementation properties, which can be written as [34]

$$v_{fb}(t) = K_p e(t) + K_i \int_0^t e(\tau)\mathrm{d}\tau, \tag{14}$$

where K_p and K_i are the proportional gain and integral gain respectively, $e(t)$ is the tracking error between the actual position and desired position. Generally, the trial-and-error method can be adopted to tune PI parameters [34]. Thus, the control voltage $v(t)$ of the closed-loop controller is expressed as

$$\begin{aligned} v(t) &= v_{ff}(t) + v_{fb}(t) \\ &= b_1' y_{\mathrm{d}}^3(t) + b_2' y_{\mathrm{d}}(t) + \sum_{i=1}^{N} q'_i F_{\mathrm{or}_i}^h[y_{\mathrm{d}}](t) \\ &\quad + K_p e(t) + K_i \int_0^t e(\tau)\mathrm{d}\tau. \end{aligned} \tag{15}$$

4. Experimental validation

In this section, an experimental platform actuated by the piezoelectric actuator is established, and experimental tests are conducted to verify the developed control schemes with the dynamic hysteresis compensator.

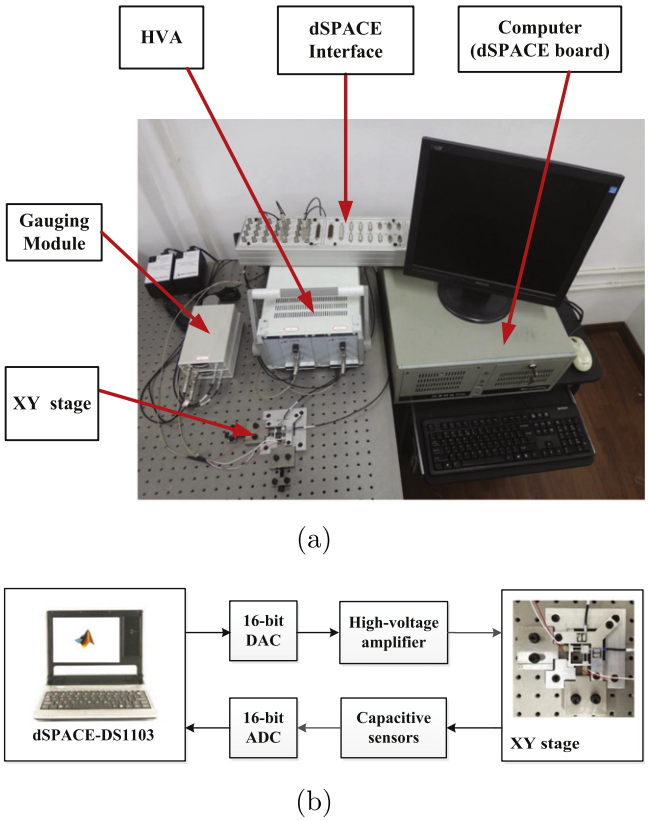

Figure 7. The experimental setup: (a) experimental platform; (b) block diagram.

Table 1. Quantified comparison of parameters in different models.

Model	Parameters' number
Ang [20] $N = 10$, $m = 4$	24
Janaideh [23] $N = 10$	23
Janaideh [24] $N = 10$, $m = 4$	16
Yang [25] $N = 10$	23
Proposed $N = 10$	14

4.1. Experimental setup

The experimental platform is shown in figure 7(a). A prototype of the *XY* stage [35] is fabricated using wire electrical discharge machining technique with aluminum 7075. The two piezoelectric actuators are mounted to drive the stage, and a dual-channel high-voltage amplifier (HVA) with a fixed gain of 20 is used to provide excitation voltage (0–200 V) for the piezoelectric actuators. Two capacitive sensors (Probe 2823 and Gauging Module 8810 from MicroSense Company (USA), range of $+/-25$ μm with analog output of $+/-$ 10 V, resolution of <1 nm-rms) are adopted to measure the displacements of the end-effector along *X*- and *Y*-axis. A dSPACE-DS1103 board equipped with the 16bit analog to digital converters and 16 bit digital to analog converters is utilized to output the excitation voltage for the HVA and capture the real-time displacement information from the capacitive sensors. The sampling frequency of the system is set to 50 kHz. The block diagram of the whole experimental setup is shown in figure 7(b).

4.2. Parameter identification

In order to implement the real-time controller, the main challenge lies on the parameter identification of the inverse MRPI model (13). The threshold values in the inverse MRPI (13) are given as

$$r_i = \frac{i-1}{N} \left\| y_d(t) \right\|_\infty, \; i = 1, 2, \ldots, N, \tag{16}$$

where N is the number of the play operators. Generally, the larger N is selected, the more precise it is to describe the inverse hysteresis loops. On the other hand, more efforts should be made in the real-time calculation of compensation signals. There is a tradeoff between the computational complexity and accuracy. In this work, N is selected as 10 for an illustration. To intuitively demonstrate the advantage of fewer parameters in the proposed hysteresis model, table 1 lists a quantified comparison with existing rate-dependent PIMs [20, 23–25] when the number of threshold N is chosen as 10.

Due to the highly nonlinear, high dimensional, non-differential and multiple constraint nature, the identification of the inverse hysteresis model is a challenging problem, and many optimization algorithms have been developed to solve this problem [36, 37]. As an illustration, the modified particle swarm optimization (MPSO) algorithm [37] is utilized to simultaneously identify all the weighting values, coefficients of the polynomial input function, and coefficients of the dynamic envelope functions with fixed threshold values r_i. The key point of the MPSO optimization is the selection of the objective function. In this work, the objective function is constructed through summation of squared errors over a range of input frequencies, which is given as:

$$\Phi(X) = \sum_{j=1}^{J} \sum_{k=1}^{K_j} W_j \left(v_j(k) - v_j{}^a(k) \right)^2, \tag{17}$$

where J denotes the number of the input frequencies in the input signal, K_j is the number of the data points at the jth frequency, $v_j(k)$ and $v_j{}^a(k)$ are the calculated voltage and the actual voltage respectively at the kth sampling time at the jth input frequency, and W_j is the weight for the jth frequency which is calculated based on the hysteresis percentage presented as

$$W_j = \frac{H_j}{H_0}, \tag{18}$$

where H_j represents the hysteresis percent at the jth frequency, and H_0 represents the hysteresis percent in the rate-independent case.

As an illustration, sinusoidal input signals with fixed amplitude (26 V) and different frequencies (10, 100, and

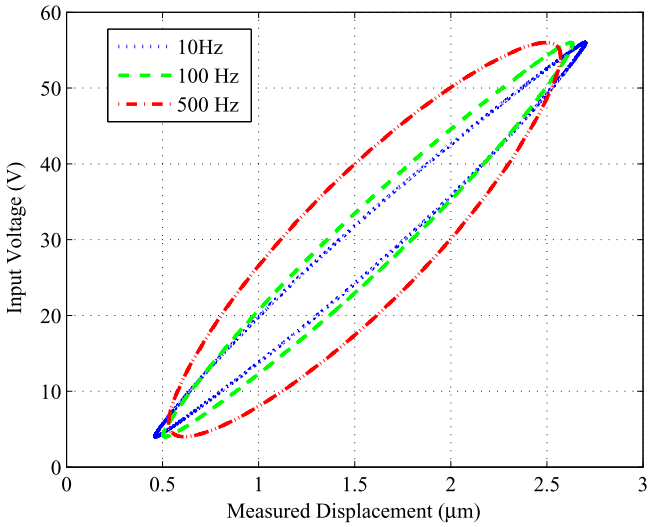

Figure 8. Relationship between the measured displacement and the input voltage at different frequencies.

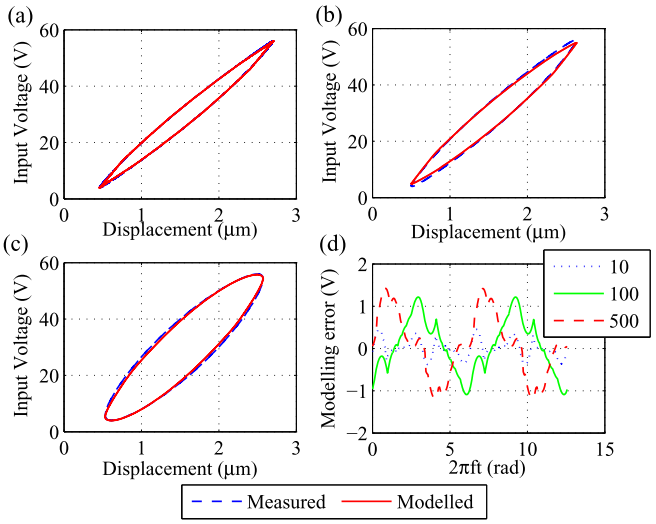

Figure 9. Comparison between the measured results and the predicted results from the identified model.

Table 2. Identified parameters of the inverse MRPI model.

i	q'_i	b'_i
1	−4.8645	0.1410
2	−0.3310	6.4714
3	−0.0668	
4	−0.1103	
5	−0.0586	
6	−0.0475	
7	−0.0790	
8	0.0303	
9	0.6290	
10	−0.6684	
α	2.1500e-05	
β	2.1217e-05	

500 Hz) are applied to the piezoelectric actuator. The relation of the measured displacement and the input voltage is shown in figure 8, which is used to identify the parameters of the inverse MRPI hysteresis model (13). From figure 8, the hysteresis percent is obtained as 16.44%,22.56%, and 45.51% for 10, 100, and 500 Hz respectively. Thus, the weights $W_j (j = 1, 2, 3)$ are calculated as 1, 1.37, and 2.77 for 10, 100, and 500 Hz respectively. Table 2 lists the identified parameters of the inverse MRPI model (13). It should be mentioned that in the proposed model, α and β are multiplied by the derivative of the input signal $\dot{y}_d(t)$, which is calculated as $(y_d(t) - y_d(t - T))/T$ with the sampling time $T = 0.00002$ s. The higher the input frequency is, the larger the derivative of the input signal $\dot{y}_d(t)$ is. In order to make sure that the values of the terms $\alpha\dot{y}_d(t)$ and $\beta\dot{y}_d(t)$ are under the same level with the input signal $y_d(t)$, the values of α and β should be selected small. Figure 9 shows the comparison between the model simulation output and the experimental data. The maximum modeling error lies within 2.7%, which demonstrates the effectiveness of the identified model.

4.3. Open-loop tracking control experiments

In order to validate the proposed MRPI model, open-loop control scheme of figure 5 is implemented. For comparison, the open-loop controllers based on the inverse MPI model (12) and the inverse WRPI model are developed, where the abbreviation of WRPI represents the rate-dependent PIM based on dynamic weighting functions $(w_i = k_i + l_i\dot{y}_d(t))$ [20]. In the developed controllers, the MPI and WRPI models are applied to directly describe inverse hysteresis loops of piezoelectric actuators using the direct inverse hysteresis compensation method, and their parameters are identified by the MPSO algorithm with the same objective function as that of the MRPI model. The identified parameters of the MPI model are summarized as: $a'_1 = 0.2993$, $a'_2 = 1.6289$, $p'_1 = -0.0569$, $p'_2 = -0.2385$, $p'_3 = -0.1977$, $p'_4 = -0.0220$, $p'_5 = -0.0702$, $p'_6 = -0.0543$, $p'_7 = -0.1039$, $p'_8 = -0.0026$, $p'_9 = -0.0028$, $p'_{10} = -0.0932$. The identified parameters of the WRPI model are summarized as: $a_1 = 0.1100$, $a_2 = 2.5503$, $k_1 = -1.0000$, $k_2 = -0.3428$, $k_3 = 0.0482$,$k_4 = -0.1649$, $k_5 = -0.0360$, $k_6 = -0.0655$, $k_7 = 0.0316$,$k_8 = -0.1539$, $k_9 = 0.3795$, $k_{10} = -1.0000$, $l_1 = 2.4093e-03$, $l_2 = -2.8561e-03$, $l_3 = 0.7293e-03$, $l_4 = -0.4161e-03$, $l_5 = 0.3174e-03$, $l_6 = -0.4613e-03$, $l_7 = 3.0950e-03$, $l_8 = -6.4515e-03$, $l_9 = 0.0129$, $l_{10} = 1.0000$.

In the experiments, a series of sinusoidal trajectories with frequencies in the range from 10 to 500 Hz are generated. figure 10 shows the tracking results of different open-loop controllers at 10 and 500 Hz. It can be observed that with the controller based on MRPI model, the actual displacement well follows the desired trajectory, which demonstrate the superiority of the dynamic hysteresis compensator based on the inverse MRPI model. To quantify the performance of open-

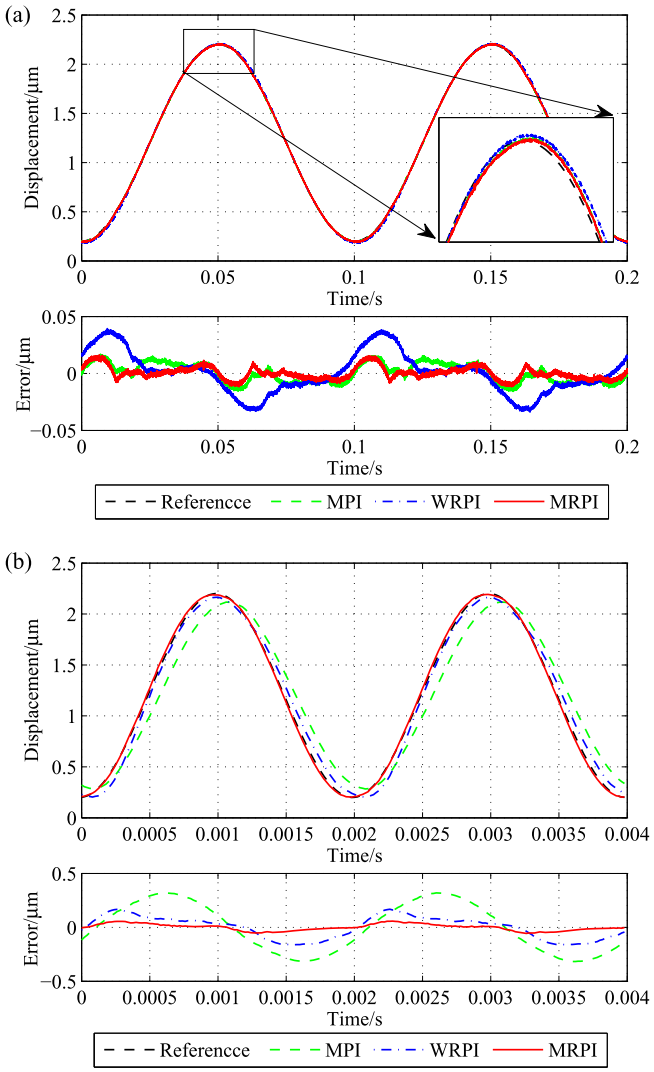

Figure 10. Time history of the sinusoidal trajectory tracking results using open-loop control: (a) 10 Hz; (b) 500 Hz.

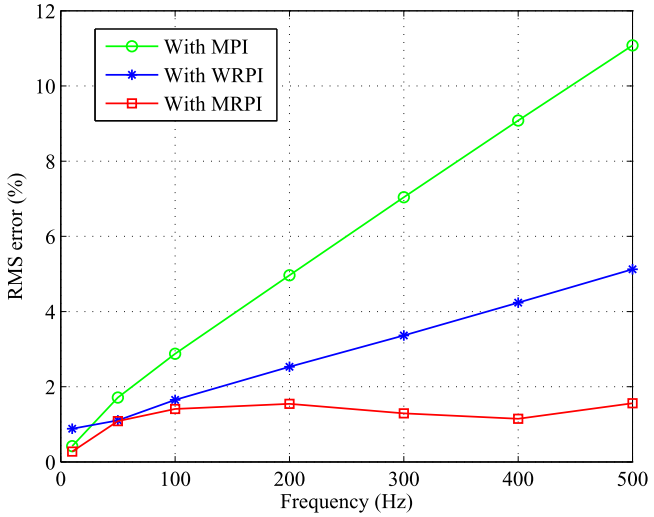

Figure 11. Comparison of the rms error with different open-loop controllers under sinusoidal inputs with frequencies from 10 to 500 Hz.

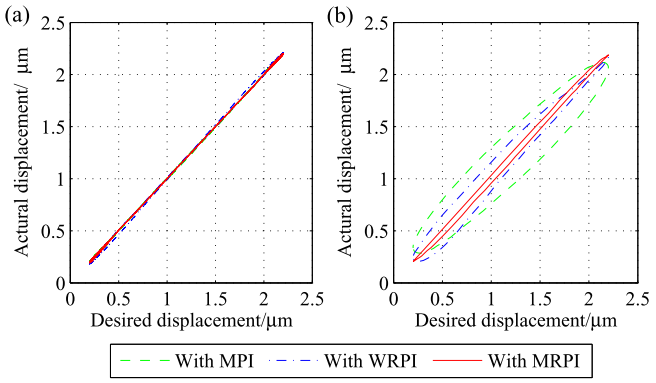

Figure 12. Hysteresis reduction via different open-loop controllers under the sinusoidal trajectory at (a) 10 Hz and (b) 500 Hz.

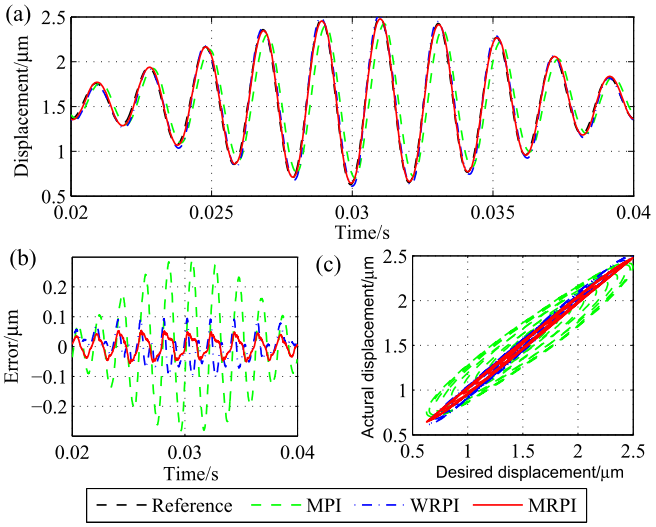

Figure 13. Comparison of the complex harmonic trajectory tracking results via various open-loop controllers: (a) time history of the displacement, (b) time history of the tracking error and (c) the input–output relation.

loop controllers, the root mean square (rms) error defined as

$$e_{\mathrm{rms}} = \frac{\sqrt{\frac{1}{n}\sum_{k=1}^{n}\left(y_{\mathrm{d}}(k) - y(k)\right)^2}}{\max_k\left(y_{\mathrm{d}}(k)\right) - \min_k\left(y_{\mathrm{d}}(k)\right)} \times 100\% \qquad (19)$$

is calculated and shown in figure 11. It is found that the rms error via dynamic hysteresis compensator with inverse MRPI model is within 1.6%, while the rms errors via hysteresis compensator with inverse MPI model and inverse WRPI model increase to 11% and 5.12% at 500 Hz respectively. The results show that a clear improvement of the tracking accuracy is achieved when using the dynamic hysteresis compensator with inverse MRPI model. In addition, in the case of hysteresis reduction, the dynamic hysteresis compensator based on inverse MRPI model can significantly reduce the hysteresis nonlinearity of piezoelectric actuators, and improve the output linearity better than the hysteresis compensator based on inverse MPI model and the dynamic

hysteresis compensator based on the inverse WRPI model, especially at high frequencies. This is demonstrated in figure 12.

To further verify the effectiveness of dynamic hysteresis compensator with the developed inverse MRPI model, experiments with complex harmonic references are conducted. Figure 13 shows the time history of the output displacement and the tracking error using the hysteresis compensators based on the inverse MPI, WRPI and MRPI models, respectively. The results demonstrate that compared to the hysteresis compensator with the inverse MPI model and the dynamic hysteresis compensator with the inverse WRPI model, the dynamic hysteresis compensator with the inverse MRPI model achieve better tracking accuracy. Figure 13 also shows the input–output relation between the desired displacement and actual displacement with the hysteresis compensators based on the inverse MPI, WRPI and MRPI models. The results demonstrate that the dynamic hysteresis compensator with inverse MRPI model is superior to the hysteresis compensators with inverse MPI and WRPI models for compensating both major and minor rate-dependent hysteresis nonlinearities.

4.4. Closed-loop tracking control experiments

A hybrid controller (see figure 6) combining a PI feedback and a dynamic hysteresis compensator based on MRPI model is tested using the same reference signal as in the open-loop tracking control experiments. For comparison, the PI, PI +MPI, and PI+WRPI controllers are also tested. In the experiments, the control gains K_p and K_i are tuned as 1 and 6000 for all the controllers. It is worthy of mentioning that these values are determined by the trial-and-error method in the experiments for the PI controller and kept unchanged for the PI+MPI, PI+WRPI, and PI+MRPI controllers.

Figure 14 shows the tracking results of the PI+MRPI controller at 10 and 500 Hz, where the actual displacement well follows the desired trajectory. Figure 14 also shows the tracking results of the PI, PI+MPI, and PI+WRPI controllers. The results demonstrate that the PI+MRPI controller achieves better tracking accuracy than the PI, PI+MPI, and PI+WRPI controllers. For quantitative comparison, the rms errors of the different closed-loop controllers are calculated and shown in figure 15. It can be observed that the rms error of the PI +MRPI controller lies within 2.3%, while the rms errors of the PI, PI+MPI, and PI+WRPI controllers are up to 37%, 12.3% and 4.5% at 500 Hz respectively. Based on these results, an obvious improvement of the closed-loop tracking accuracy is achieved when using the PI+MRPI controller. figure 16 shows the input–output relation between the desired displacement and actual displacement with different closed-loop controllers. The results show that the PI+MRPI controller can significantly reduce the hysteresis nonlinearities compared with the PI, PI+MPI, and PI+WRPI controllers, especially at the high frequencies.

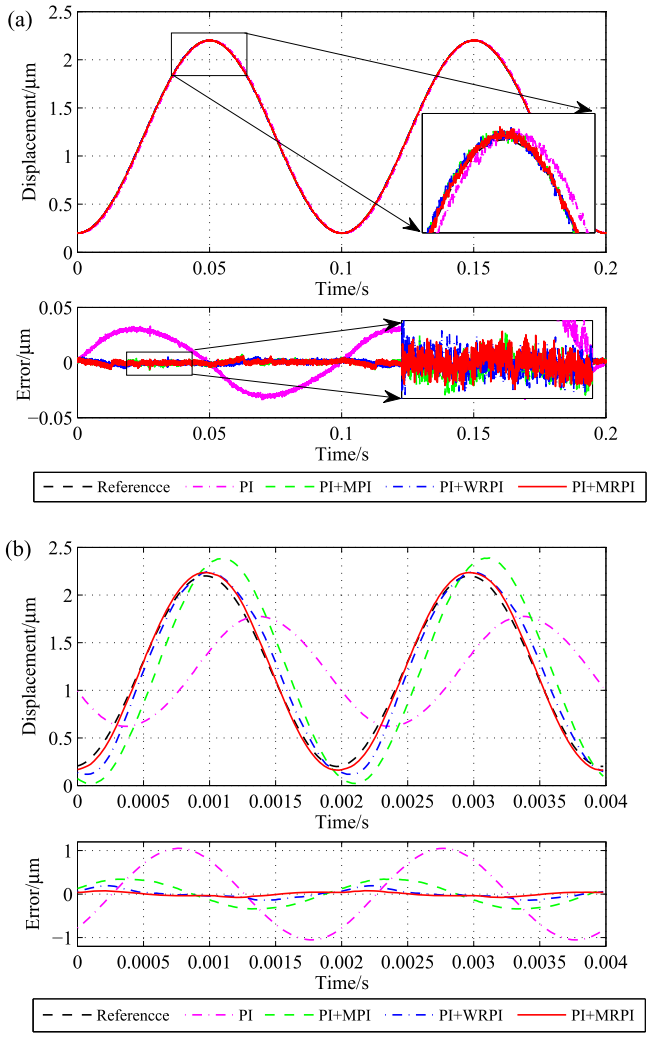

Figure 14. Time history of the sinusoidal trajectory tracking results using closed-loop control: (a) 10 Hz; (b) 500 Hz.

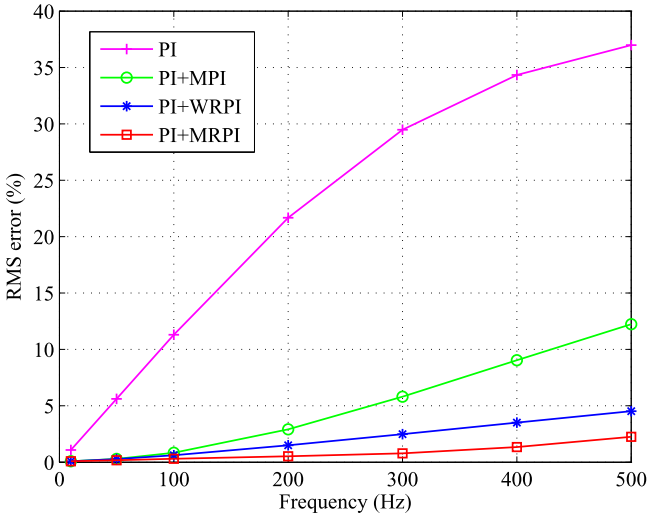

Figure 15. Comparison of the rms error with different closed-loop controllers under sinusoidal inputs with frequencies from 10 to 500 Hz.

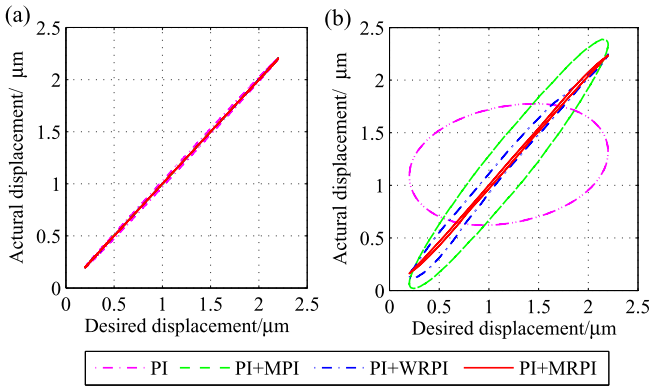

Figure 16. Hysteresis reduction via different closed-loop controllers under the sinusoidal trajectory at (a) 10 Hz and (b) 500 Hz.

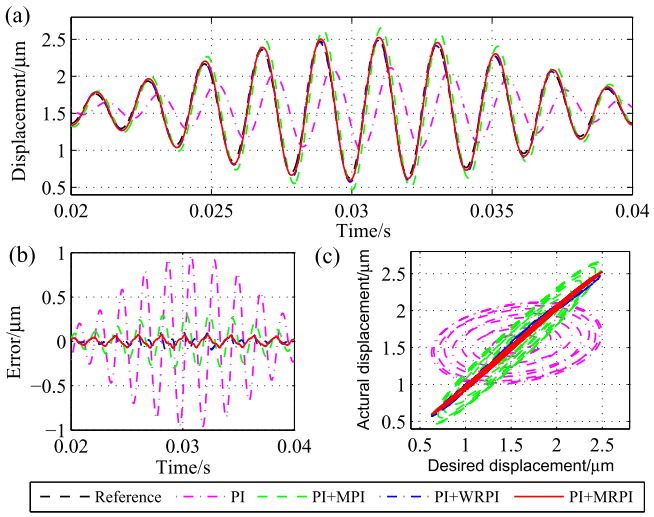

Figure 17. Comparison of the complex harmonic trajectory tracking results via various closed-loop controllers: (a) time history of the displacement, (b) time history of the tracking error and (c) the input–output relation.

Experiments with complex harmonic references are also conducted to verify the effectiveness of the PI+MRPI controller. Figure 17 shows the time history of the output displacement and tracking error with the PI, PI+MPI, PI +WRPI, and PI+MRPI controllers. The results demonstrate that the PI+MRPI control is the best algorithm in terms of tracking accuracy. Figure 17 also shows the input–output relation between the desired displacement and actual displacement. The results demonstrate that the PI+MRPI controller is superior to the PI, PI+MPI, and PI+WRPI controllers for compensating both major and minor rate-dependent hysteresis nonlinearities.

The experimental results indicate that the combination of feedback and feedforward can achieve a better performance compared with those cases with feedback or feedforward alone. However, the feedback loop does not always improve the tracking performance. As shown in figures 11 and 15, the feedback controller improves the tracking precision when the input frequency is lower than 400 Hz, and causes the tracking performance to deteriorate at sufficiently high frequencies,

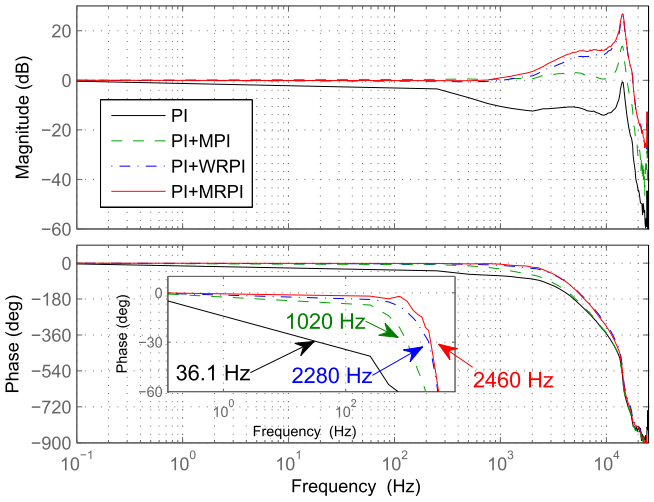

Figure 18. Control bandwidth results of the nanopositioning stage with PI, PI+MPI, PI+WRPI, and PI+MRPI controllers.

i.e., 500 Hz. Therefore, it is better to use the feedforward only when the input frequency exceeds a certain value.

Finally, a band-limit white noise signal is applied to test the controllers' bandwidth. Figure 18 shows the frequency responses of the PI, PI+MPI, PI+WRPI, and PI+MRPI controllers. It is observed that the ordinary −3 dB bandwidth corresponds to large phase lags. Hence, the 30°-lag control bandwidth defined as the frequency at which the phase is lagged 30° is adopted in this paper. The 30°-lag control bandwidths of the PI, PI+MPI, PI+WRPI, and PI+MRPI controllers are 36.1 Hz, 1020 Hz, 2280 Hz, and 2460 Hz, respectively. By adding the feedforward hysteresis compensator, the bandwidth of the controller is significantly increased. However, some of the bandwidth is uncontrolled due to the lightly damped resonance. Therefore, the damping control approach is necessary to suppress the resonance, which will be further investigated in the future works.

5. Conclusion

In this paper, a MRPI model is proposed to characterize the rate-dependent asymmetric hysteresis nonlinearity of piezoelectric actuators, which is constructed by employing dynamic envelope functions into the MPI model. The benefit of the developed MRPI model lies in the fact that it has a relatively simple mathematic format with fewer parameters to describe the rate-dependent asymmetric hysteresis behavior, and all the parameters of the model can be identified simultaneously without any postprocessing. In addition, available control approaches can be directly adopted with the developed MRPI model for the hysteresis compensation of the piezoelectric actuators. On this basis, an inverse dynamic hysteresis compensation method is presented to enhance the tracking accuracy of piezo-actuated nanopositioning stages exhibiting rate-dependent hysteresis behavior. The proposed method utilizes the developed MRPI model to directly describe the inverse hysteresis effect of piezoelectric

actuators. The parameters of the inverse MRPI model are identified directly from the experimental data using the MPSO algorithm. The maximum modeling error of the inverse MRPI model is 2.7%, which demonstrates the effectiveness of the identified model. Then, a new open-loop tracking controller based on the inverse dynamic hysteresis compensator is developed and assessed when a sinusoidal reference signal with frequencies from 10 to 500 Hz and a complex harmonic reference are applied to the piezoelectric actuators, respectively. A closed-loop controller, with PI plus a feedforward dynamic hysteresis compensator, is also designed and tested using the same reference signals. Experimental results show that the tracking accuracy of the controllers with MRPI model is greatly improved compared to those of the controllers with the MPI model and the WRPI model.

Acknowledgments

This work was supported by the National Natural Science Foundation of China under Grant Nos. 51405293 and 51421092, and the Specialized Research Fund for the Doctoral Programme of Higher Education under Grant No. 20130073110037.

References

[1] Yong Y K, Moheimani S O R, Kenton B J and Leang K K 2012 Invited review article: high-speed flexure-guided nanopositioning: mechanical design and control issues *Rev. Sci. Instrum.* **83** 121101

[2] Li Y and Xu Q 2011 A novel piezoactuated XY stage with parallel, decoupled, and stacked flexure structure for micro-/nanopositioning *IEEE Trans. Ind. Electron.* **58** 3601–15

[3] Przybylski J 2009 Nonlinear vibrations of a beam with a pair of piezoceramic actuators *Eng. Struct.* **31** 2687–95

[4] Xu Q 2013 Adaptive discrete-time sliding mode impedance control of a piezoelectric microgripper *IEEE Trans. Robot.* **29** 663–73

[5] Tian Y L, Zhang D and Shirinzadeh B 2011 Dynamic modelling of a flexure-based mechanism for ultra-precision grinding operation *Precis. Eng.* **35** 554–65

[6] Mrad B and Hu H R 2002 A model for voltage-to-displacement dynamics in piezoceramic actuators subject to dynamic-voltage excitations *IEEE Trans. Mechatronics* **7** 479–89

[7] Hu H, Georgiou H M S and Ben-Mrad R 2005 Enhancement of tracking ability in piezoceramic actuators subject to dynamic excitation conditions *IEEE Trans. Mechatronics* **10** 230–9

[8] Croft D, Shed G and Devasia S 2001 Creep, hysteresis, and vibration compensation for piezoactuators: atomic force microscopy application *Trans. ASME, J. Dyn. Syst. Meas. Control* **123** 35–43

[9] Song G, Zhao J, Zhou X and Abreu-García J 2005 Tracking control of a piezoceramic actuator with hysteresis compensation using inverse Preisach model *IEEE Trans. Mechatronics* **10** 198–209

[10] Li Z, Su C Y and Chai T 2014 Compensation of hysteresis nonlinearity in magnetostrictive actuators with inverse multiplicative structure for Preisach model *IEEE Trans. Autom. Sci. Eng.* **11** 613–9

[11] Rakotondrabe M 2011 Bouc–Wen modeling and inverse multiplicative structure to compensate hysteresis nonlinearity in piezoelectric actuators *IEEE Trans. Autom. Sci. Eng.* **8** 428–31

[12] Xu Q and Li Y 2010 Dahl model-based hysteresis compensation and precise positioning control of an XY parallel micromanipulator with piezoelectric actuation *Trans. ASME, J. Dyn. Syst. Meas. Control* **132** 041011

[13] Kuhnen K 2003 Modeling, identification and compensation of complex hysteretic nonlinearities: a modified Prandtl–Ishlinskii approach *Eur. J. Control* **9** 407–18

[14] Liu S and Su C Y 2011 A note on the properties of a generalized Prandtl–Ishlinskii model *Smart Mater. Struct.* **20** 087003

[15] Shan Y and Leang K K 2012 Dual-stage repetitive control with Prandtl–Ishlinskii hysteresis inversion for piezo-based nanopositioning *Mechatronics* **22** 271–81

[16] Gu G Y, Zhu L M and Su C Y 2014 Modeling and compensation of asymmetric hysteresis nonlinearity for piezoceramic actuators with a modified Prandtl–Ishlinskii model *IEEE Trans. Ind. Electron.* **61** 1583–95

[17] Xiao S and Li Y 2013 Modeling and high dynamic compensating the rate-dependent hysteresis of piezoelectric actuators via a novel modified inverse Preisach model *IEEE Trans. Control Syst. Technol.* **21** 1549–57

[18] Li W, Chen X and Li Z 2013 Inverse compensation for hysteresis in piezoelectric actuator using an asymmetric rate-dependent model *Rev. Sci. Instrum.* **84** 115003

[19] Xiao S and Li Y 2014 Dynamic compensation and H_∞ control for piezoelectric actuators based on the inverse Bouc–Wen model *Robot. Comput.-Integr. Manuf.* **30** 47–54

[20] Ang W T, Khosla P K and Riviere C N 2007 Feedforward controller with inverse rate-dependent model for piezoelectric actuators in trajectory-tracking applications *IEEE/ASME Trans. Mechatronics* **12** 134–42

[21] Tan U X, Latt W T, Widjaja F, Shee C Y, Riviere C N and Ang W T 2009 Tracking control of hysteretic piezoelectric actuator using adaptive rate-dependent controller *Sensors Actuators* A **150** 116–23

[22] Qin Y, Shirinzadeh B, Tian Y and Zhang D 2013 Design issues in a decoupled XY stage: static and dynamics modeling, hysteresis compensation, and tracking control *Sensors Actuators* A **194** 95–105

[23] Janaideh M A, Su C Y and Rakheja S 2008 Development of the rate-dependent Prandtl–Ishlinskii model for smart actuators *Smart Mater. Struct.* **17** 035026

[24] Janaideh M A and Krejčí P 2013 Inverse rate-dependent Prandtl–Ishlinskii model for feedforward compensation of hysteresis in a piezomicropositioning actuator *IEEE/ASME Trans. Mechatronics* **18** 1498–507

[25] Yang M J, Li C X, Gu G Y and Zhu L M 2014 A modified Prandtl–Ishlinskii model for rate-dependent hysteresis nonlinearity using mth-power velocity damping mechanism *Int. J. Adv. Robot. Syst.* **11** 163

[26] Tsai M-S and Chen J-S 2003 Robust tracking control of a piezoactuator using a new approximate hysteresis model *Trans. ASME, J. Dyn. Syst. Meas. Control* **125** 96–102

[27] Gu G and Zhu L 2010 High-speed tracking control of piezoelectric actuators using an ellipse-based hysteresis model *Rev. Sci. Instrum.* **81** 085104

[28] Hong R, Tan Y, Chen H and Xie Y 2008 A neural networks based model for rate-dependent hysteresis for piezoceramic actuators *Sensors Actuators* A **143** 370–6

[29] Wong P K, Xu Q, Vong C M and Wong H C 2012 Rate-dependent hysteresis modeling and control of a piezostage using online support vector machine and relevance vector machine *IEEE Trans. Ind. Electron.* **59** 1988–2001

[30] Xu Q 2013 Identification and compensation of piezoelectric hysteresis without modeling hysteresis inverse *IEEE Trans. Ind. Electron.* **60** 3927–37

[31] Li P, Yan F, Ge C, Wang X, Xu L, Guo J and Li P 2013 A simple fuzzy system for modelling of both rate-independent and rate-dependent hysteresis in piezoelectric actuators *Mech. Syst. Signal Process.* **36** 182–92

[32] Gu G Y, Yang M J and Zhu L M 2012 Real-time inverse hysteresis compensation of piezoelectric actuators with a modified Prandtl–Ishlinskii model *Rev. Sci. Instrum.* **83** 065106

[33] Janocha H and Kuhnen K 2000 Real-time compensation of hysteresis and creep in piezoelectric actuators *Sensors Actuators* A **79** 83–9

[34] Ge P and Jouaneh M 1996 Tracking control of a piezoceramic actuator *IEEE Trans. Control Syst. Technol.* **4** 209–16

[35] Li C X, Gu G Y, Yang M J and Zhu L M 2013 Design, analysis and testing of a parallel-kinematic high-bandwidth XY nanopositioning stage *Rev. Sci. Instrum.* **84** 125111

[36] Chan C H and Liu G J 2007 Hysteresis identification and compensation using a genetic algorithm with adaptive search space *Mechatronics* **17** 391–402

[37] Yang M J, Gu G Y and Zhu L M 2013 Parameter identification of the generalized Prandtl–Ishlinskii model for piezoelectric actuators using modified particle swarm optimization *Sensors Actuators* A **189** 254–65